DFT/TDDFT study on the electronic structure and spectral properties in annulated analogue of phenyl heteroazulene derivative

ARTICLE *in* MATERIALS CHEMISTRY AND PHYSICS · FEBRUARY 2012

Impact Factor: 2.26 · DOI: 10.1016/j.matchemphys.2011.11.025

7 AUTHORS, INCLUDING:

Krzysztof S Danel
University of Agriculture in Krakow
40 PUBLICATIONS **527** CITATIONS
SEE PROFILE

Marek Matusiewicz
Czestochowa University of Technology
23 PUBLICATIONS **132** CITATIONS
SEE PROFILE

Tomasz Uchacz
Jagiellonian University
26 PUBLICATIONS **170** CITATIONS
SEE PROFILE

Andriy V. Kityk
Czestochowa University of Technology
206 PUBLICATIONS **1,935** CITATIONS
SEE PROFILE

Materials Chemistry and Physics 132 (2012) 330–338

Contents lists available at SciVerse ScienceDirect

Materials Chemistry and Physics

journal homepage: www.elsevier.com/locate/matchemphys

DFT/TDDFT study on the electronic structure and spectral properties in annulated analogue of phenyl heteroazulene derivative

P. Gąsiorski[a], K.S. Danel[b], M. Matusiewicz[a], T. Uchacz[c], W. Kuźnik[d], Ł. Piątek[a], A.V. Kityk[a,*]

[a] Faculty of Electrical Engineering, Częstochowa University of Technology, Al. Armii Krajowej 17, 42-200 Częstochowa, Poland
[b] Department of Chemistry, University of Agriculture, Balicka Str. 122, 30-149 Kraków, Poland
[c] Faculty of Chemistry, Jagiellonian University, Ingardena Str. 3, 30-060 Kraków, Poland
[d] Chemical Department, Silesian University of Technology, Strzody 9, Gliwice, Poland

ARTICLE INFO

Article history:
Received 18 April 2011
Received in revised form 6 September 2011
Accepted 13 November 2011

Keywords:
Optical absorption spectra
Fluorescence spectra
DFT and TDDFT calculations
Annulated heteroazulene dyes

ABSTRACT

Paper reports the DFT/TDDFT study on the electronic structure and spectral properties of the seven-membered annulated heteroazulene derivative 6-phenyl-6*H*-5,6,7-triazadibenzo[*f*,*h*]naphtho[3,2,1-*cd*]azulene (PTNA) by means of polarizable continuum model (PCM) and Lippert–Mataga–Onsager reaction field (LM-ORF) model at the B3LYP/6-31+G(d,p) level of theory. The results of calculations are compared with the measured optical absorption and fluorescence spectra as well as with the cyclic voltammetry data. The DFT/TDDFT methods exhibit rather good quantitative agreement regarding the spectral position of the first absorption band; the discrepancy between the experiment and theory is less than 0.1 eV. As for the fluorescence emission the TDDFT calculations underestimate the transition energy of about 0.45 eV. The discrepancy should be attributed to insufficient accuracy of the TDDFT optimization in the excited state. In the polar solvent environment, all the TDDFT/PCM approaches give the bathochromic (red) shift for the fluorescence emission and the hypsochromic (blue) shift for the optical absorption in accordance with the experimental observation. As for the fluorescence emission fairly good agreement with the experiment provides the hybrid approach being the combination of the TDDFT/PCM optimization with the semiempirical electronic structure calculations by PM3 method and solvation LM-ORF model predicting the emission energy in different solvents with the accuracy better than 0.06 eV.

1. Introduction

Seven-membered cyclization of triphenyl pyrazoloquinoline derivatives into regioisomers of annulated heteroazulenes provides a significant red shift of their electronic absorption and emission spectra [1–4]. Fundamental interest to such phenomena is also accompanied by practical needs in novel fluorescent dyes suitable for efficient electroluminescence applications in blue-yellow region of the visible spectra as the dopants of polymer matrixes in electroluminescent displays and OLEDs [5–8], photovoltaic devices [9] or potentially promising ligands for triplet emitters (phosphors) [10]. Several recent works [1–4,11] reported the synthesis of the annulated heteroazulenes likewise their optical absorption and fluorescence spectra measured in the organic solvents of different polarity. A characteristic feature of these dyes is opposite solvatochromism for the optical absorption and fluorescence. The hypsochromic (blue) shift of the first absorption band is accompanied by the bathochromic (red) shift of the fluorescence band. Such behavior indeed appears to be consistent with the Lippert–Mataga solvatochromic model based on semiempirical evaluations (model PM3) which explains the opposite solvatochromism by a specific orientation of the ground and excited state dipole moments. As for the first optical absorption band the semiempirical approach [1–4] also gives a proper magnitude of its hypsochromic shift. However, similar quantitative evaluations evidently fail in the case of the bathochromic shift related with the fluorescence emission. In particular, the analysis of the fluorescence spectra measured in solvents of different polarity suggests much larger dipole moment of the lowest excited state comparing to the one obtained within the semiempirical calculations. Corresponding discrepancy may be attributed to the mixing of the excited electronic states in solvent environment and/or conformational relaxation of the solute in the excited state. Both mechanisms may indeed result in increase of the dipole moment of the lowest excited state. Evidently this problem could not be solved within the semiempirical approach itself basically due to its low efficiency in the optimization of the excited state geometry both in vacuo (gas phase) and solvent environment. Much more powerful techniques in this respect represent density

* Corresponding author.
E-mail address: kityk@ap.univie.ac.at (A.V. Kityk).

0254-0584/$ – see front matter © 2011 Elsevier B.V. All rights reserved.
doi:10.1016/j.matchemphys.2011.11.025

functional theory (DFT) and its counterpart, time-dependent DFT (TDDFT) method, combined with different types of polarizable continuum models (PCMs) or Onsager reaction field (ORF) approaches that account for an influence of the solvent shell on the solute electron structure in the ground and excited states.

In this paper we report a DFT/TDDFT/PCM/ORF study of the solvatochromic effect in one of the simplest phenyl derivatives of annulated heteroazulenes, i.e. 6-phenyl-6*H*-5,6,7-triazadibenzo[*f*,*h*]naphtho[3,2,1-*cd*]azulene (hereafter PTNA) with the chemical structure as shown below:

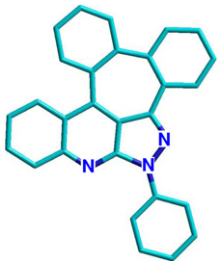

The structure PTNA is characterized by nonplanar distortion of the aromatic rings imposed by steric hindrance of interacting hydrogen atoms. Recent optical spectroscopy studies of these compounds [2] are completed in present work by cyclic voltammetry measurements directly providing the absolute energies of the HOMO and LUMO levels. The optical absorption, fluorescence and cyclic voltammetry data are compared with the results of quantum-chemical calculations. The goal behind this study is to analyze the change of the electronic structure caused by solvent-modified electron transfer interactions. In spite of previous semiempirical studies [1–3] special attention is also paid to the geometry relaxation in the excited state likewise the fluorescence emission followed by it.

2. Calculation procedure

The DFT calculations have been performed within the quantum chemical package of programs Gaussian-09 [12] using hybrid exchange-correlation (xc) potential B3LYP with the standard 6-31+G(d,p) basis set. The excitation and emission spectra likewise the dipole moments of the excited states have been calculated by means of TDDFT method. To account for the solvent influence on the solute molecular and electronic structure the DFT or TDDFT methods have been combined with ORF model or PCM. The latter one represents so-called self consistent reaction field (SCRF) approach in which the cavity is created via a set of overlapping spheres covering the individual atoms of the solute. This approach differs from the one used in several recent works [1–4,13,14] where the solute was placed in a spherical Onsager cavity within the solvent reaction field, i.e. ORF model. The geometrical optimization in the ground and excited states has been performed by DFT/PCM and TDDFT/PCM methods, respectively. The electronic transition energies and oscillator strengths at the excitation or emission processes have been calculated by TDDFT method in combination with PCM basing on two different approaches available in Gaussian-09. In the standard PCM approximation (called hereafter as PCM-LR) the vertical excitation with a linear response of solvation is considered. More advanced, so-called state-specific PCM (hereafter PCM-SS) takes into account state-specific solvation of the vertical excitation [15,16]. Further details regarding these methods are given elsewhere, see review [17] and references in. Both PCM-LR and PCM-SS approaches have been used in the combined PCM/TDDFT calculations for the solute molecule in solvents of different polarity, particularly a weakly polar cyclohexane (CHX), medium polar tetrahydrofuran (THF) and strongly polar acetonitrile (ACN). For the calculations in the gas phase standalone procedures based on DFT or TDDFT approaches have been applied.

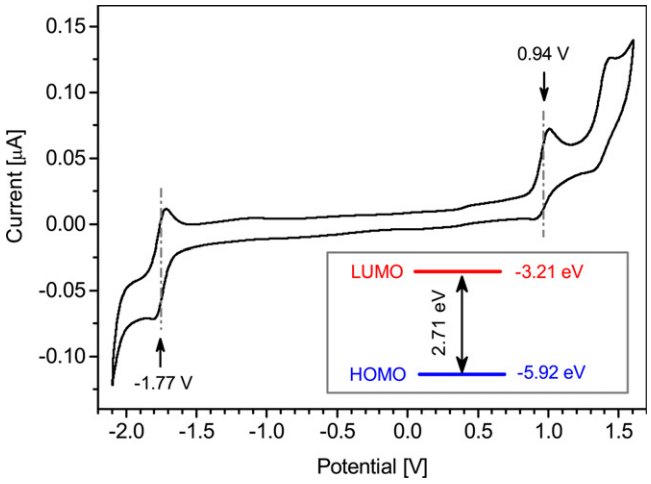

Fig. 1. Cyclic voltammogram of PTNA recorded in acetonitrile solution with respect to ferrocene redox couple. Reduction and oxidation peaks are marked by arrows. Insert shows the HOMO–LUMO levels as determined from the reduction and oxidation peaks.

The semiempirical method (PM3, Hyperchem-8.0) has been only used in the calculations of the electronic transitions (absorption and emission spectra) likewise evaluations of the excited state dipole moments. In spite of previous semiempirical studies [1–4] the molecular structure optimized within the DFT/PCM or TDDFT/PCM has been used as the input geometry in further semiempirical calculations. The solvation at such analysis has been accounted for the simple ORF model. The electronic states have been calculated using the configuration interaction (CI) method limited by orbital criterium, 24 occupied and 24 unoccupied orbitals. Further details regarding the semiempirical analysis can be found in Refs. [18–21].

3. Results and discussion

Cyclic voltammetry measurements were performed by means of AUTOLAB PGSTAT20 potentiostat–galvanostat (EcoChemie, Netherlands). The platinum and silver wires (Ø1 mm) were used as working and quasi-reference electrodes, respectively, while the platinum coil served as an auxiliary one. The potential of quasi-reference electrode was calibrated using the ferrocene as an internal standard. 0.2 M solution of Bu_4NBF_4 (Aldrich, 98% pure) in acetonitrile (POCh, 99.8% HPLC grade) was used as the electrolyte. Prior to the measurements the solution was purged with argon to remove residual oxygen. The measurement consists of determining the ferrocene redox pair potential with respect to free electron in vacuum at rest [22,23]. In the following the oxidation and reduction potentials with respect to the ferrocene redox pair were recalculated into the HOMO and LUMO energy levels. The measured voltammogram is depicted in Fig. 1. The oxidation and reduction peaks associated with the HOMO and LUMO levels, respectively, are marked in this plot by the arrows. The HOMO energy level, E_H, was estimated from a known linear relationship with the oxidation potential [24]: $E_H = -(1.4 \pm 0.1) \times qV_{CV} - (4.6 \pm 0.08)$ eV, where qV_{CV} is the oxidation potential with respect to ferrocene redox couple. This empirical expression is also supported by solid theoretical investigation. The LUMO energy level, E_L, was obtained by adding the energy of the HOMO–LUMO gap, ΔE_{HL}, to E_H value, while the energy gap ΔE_{HL} was determined from the difference between oxidation and reduction potentials. It turns out that PTNA exhibits the HOMO level at −5.92 eV and the LUMO level at −3.21 eV with the

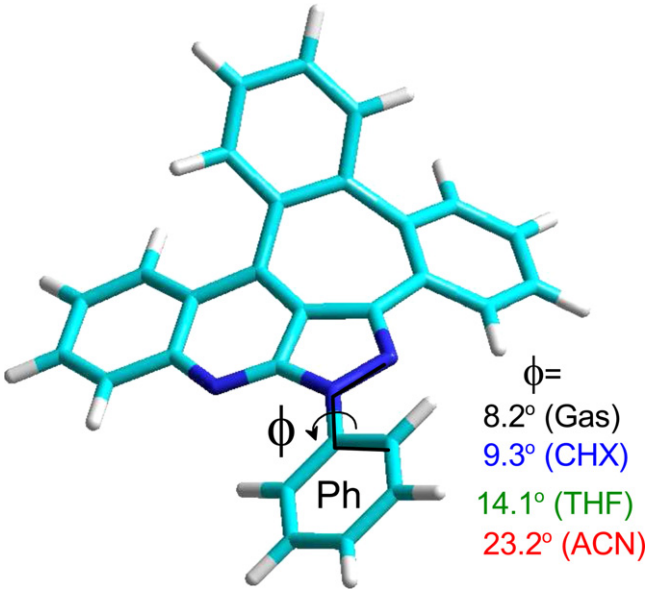

Fig. 2. Ground state equilibrium geometry of PTNA molecule in the gas phase or CHX, THF and ACN solutions as optimized by DFT or DFT/PCM methods, respectively. The overall shape of the heteroazulene moiety remains practically unchanged with the solvent polarity. Only the angular orientation of the phenyl group, characterized by the torsion angle ϕ, demonstrates evident changes toward more twisted orientations as the solvent polarity rises.

HOMO–LUMO gap ΔE_{HL} of 2.71 eV, see energy diagram in insert of Fig. 1.

Fig. 2 shows the equilibrium ground state geometry of the PTNA molecule optimized by DFT/PCM. The overall shape of the molecule as well as the bond lengths changes insignificantly (less than 0.001 Å) with the solvent polarity. Only the angular orientation of the phenyl group, characterized by the torsion angle ϕ, demonstrates evident changes starting from $\phi = 8.2^\circ$, as for the gas phase, toward more twisted orientations while the polarity rises from CHX ($\phi = 9.3^\circ$) to ACN ($\phi = 23.2^\circ$).

Fig. 3 presents the HOMO and LUMO orbitals (gas phase, reproduced by means of the program Gabedit [25]) as well as the energy diagrams calculated by DFT/PCM in solvents of different polarity in the equilibrium ground state (a) or excited state (b) geometry, which is relevant with the vertical absorption or emission processes, respectively. The HOMO → LUMO transition at the vertical excitation, likewise the reverse LUMO → HOMO transition due to the vertical emission, exhibits only a moderate change in the charge distribution without its evident separation being rather a characteristic feature of local transitions. Both HOMO and LUMO levels lower down as the solvent polarity rises. However, for the excitation process the HOMO energy decreases faster than LUMO one resulting thereby in increase of the HOMO–LUMO gap. The situation is just opposite for the fluorescence emission where the HOMO–LUMO gap shrinks on rising solvent polarity. Obviously, such opposite trends appear in agreement with the blue shift of the first absorption band and the red shift of the emission band observed in the measured optical absorption and fluorescence spectra, respectively, see Figs. 4(a), 5 and 7(a). Our quantum-chemical analysis shows that both emission or absorption processes are caused by electronic transitions between the singlet ground state, S_0, and the lowest excited state, S_1, consisting mainly from the HOMO ⇆ LUMO transition. The vertical excitation takes place here in the solvent reaction field corresponding to the ground state geometry, which stabilizes evidently better the equilibrium ground state S_0 rather than the non-equilibrium excited state S_1. At the fluorescence emission vice versa, the reaction

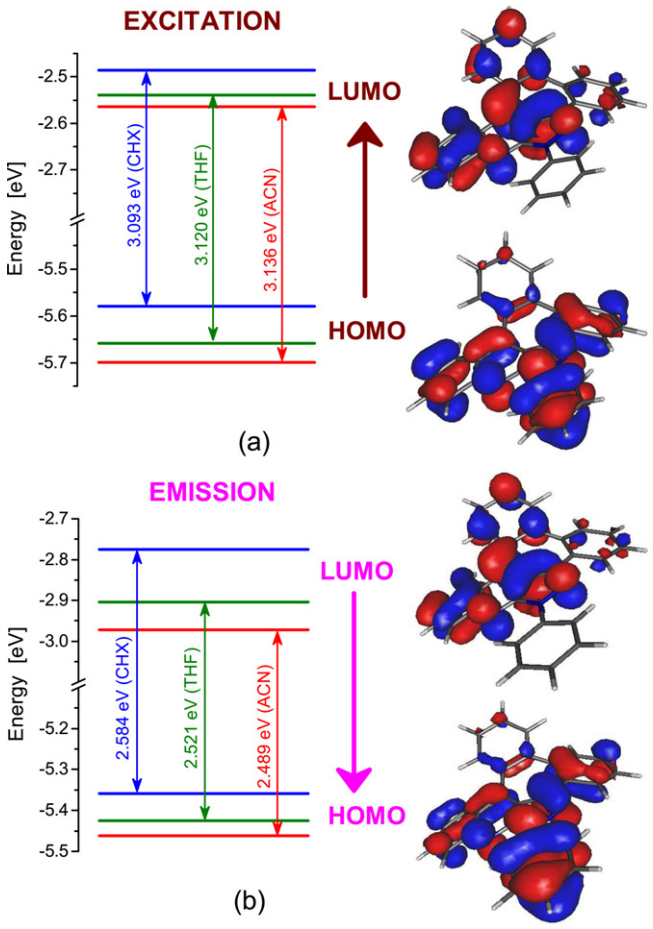

Fig. 3. HOMO and LUMO orbitals of PTNA as calculated by DFT method in the gas phase (right). HOMO and LUMO energy levels calculated by the DFT/PCM method in CHX (blue), THF (green) and ACN (red) solutions (left). (a) and (b) correspond to excitation and emission processes, respectively. The molecular geometries have been optimized by DFT/PCM (excitation, equilibrium ground state S_0) and TDDFT/PCM (emission, equilibrium excited state S_1) methods. (For interpretation of the references to color in this figure legend, the reader is referred to the web version of the article.)

solvent field induced by a relaxed excited solute stabilizes better the equilibrium excited state S_1 rather than the non-equilibrium final ground state S_0. Quantitatively, the HOMO and LUMO levels calculated in polar solvents, e.g. ACN, may be in principle compared with the results of cyclic voltammetry measurements. The calculations give the energies of the HOMO and LUMO levels (−5.70 eV and −2.56 eV, respectively) being somewhat higher compared to the measured ones (−5.92 eV and −3.21 eV, respectively) likewise also for the HOMO–LUMO gap itself, 3.14 eV (calculation) against 2.71 eV (experiment). Such discrepancy may be attributed to the tolerance of the electrochemical measurements as well as the accuracy of the DFT/PCM calculations, basically due to a "static" feature of the DFT method. This appears to be especially crucial in estimation of the HOMO–LUMO gap associated with the electronic transitions in redox, optical absorption or emission processes. One should be emphasized that DFT method calculates the virtual and occupied molecular orbitals (MOs) in the ground state being suitable mainly for a crude evaluation of the electronic transition energies likewise the trends related to their changes in a solvent environment. In this respect more appropriate is TDDFT method which mixes pairs of MOs due to correlation effects. Within such calculations one deals with so-called occupied and unoccupied natural transition orbitals (NTOs) [26] corresponding to the electron and hole states for each given excitation, respectively. Obviously,

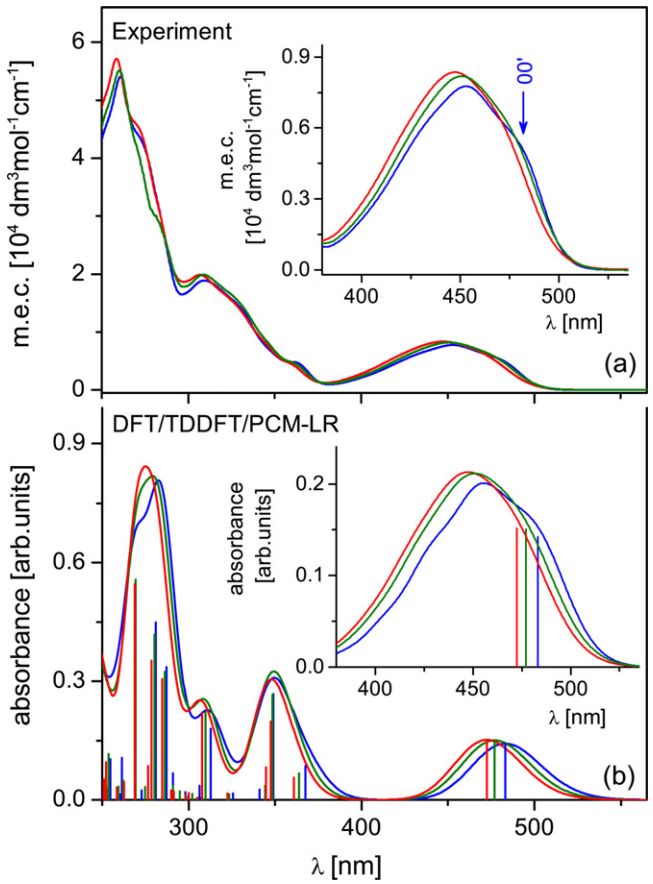

Fig. 4. The optical absorption spectra of PTNA. (a) The measured spectra in CHX (blue), THF (green) and ACN (red) solutions; insert shows the first absorption band in detail. (b) The calculated spectra by DFT/TDDFT/PCM-LR in CHX (blue), THF (green) and ACN (red) solutions. The vertical lines are the oscillator strengths corresponding to the electronic transitions between the ground and excited singlet states ($\Gamma = 0$); the continuous lines simulate the optical absorption spectra by introducing the Gaussian lineshape broadening ($\Gamma = 0.25$ eV). The inserts in (b) show the first absorption band calculated by means of Eq. (3) in CHX, THF and ACN solutions (see text for corresponding details). (For interpretation of the references to color in this figure legend, the reader is referred to the web version of the article.)

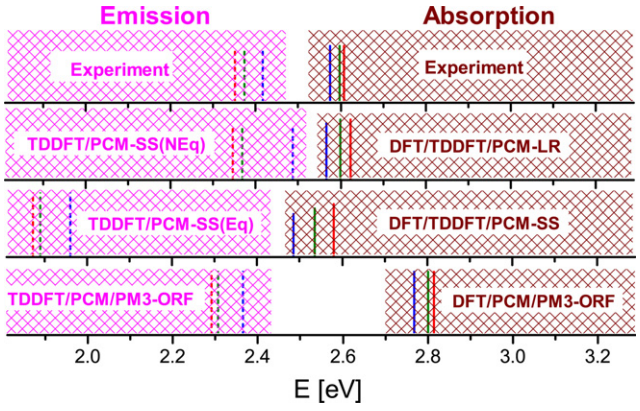

Fig. 5. Spectral positions of the first absorption bands ($0 \rightarrow 0'$ transition, vertical solid lines, right subsection) and fluorescent bands ($0' \rightarrow 0$ transition, vertical dashed lines, left subsection) being determined from the measured spectra and calculated within several approaches as specified by labels. Calculations relevant with the equilibrium or non-equilibrium states of the solute (as for the fluorescence emission only) are marked as Eq or NEq, respectively. Blue, green or red color corresponds to CHX, THF or ACN solutions, respectively. (For interpretation of the references to color in this figure legend, the reader is referred to the web version of the article.)

occupied and unoccupied NTOs are not the same as virtual and occupied MO pairs obtained within the ground state calculations [27].

The optical absorption spectrum of PTNA is unstructured in highly and medium polar solvents (see Fig. 4(a)). However, a certain structuring with strongly overlapped vibronic bands, equally spaced by approximately 1300 cm^{-1}, is evidently presented in the first optical absorption band for the spectrum measured in weakly polar solvents, e.g. CHX. The first absorption maximum is centered at about 453 nm although the electronic $0 \rightarrow 0'$ transition, associated with the HOMO–LUMO transition, should be assigned to the kink-like shoulder observed at about 481 nm at the red wing of this band, see marked by the arrow in insert of Fig. 4(a). Accordingly, the HOMO–LUMO gap obtained by the optical absorption method [$\Delta E_{HL} = 2.58$ eV (CHX), $\Delta E_{HL} = 2.61$ eV (ACN)], which is of about 0.1 eV smaller compared to the one measured by the cyclic voltammetry ($\Delta E_{HL} = 2.71$ eV), basically well agrees with the TDDFT calculations. In particular, Fig. 5 compares the spectral positions of the first absorption band (0–0′ transition) and fluorescence band (emission maxima) as determined from the spectral measurements and calculated within several approaches. Herein DFT/TDDFT/PCM-LR or DFT/TDDFT/PCM-SS represents standard electronic structure calculations, i.e. the combinations of the DFT method (geometry optimization in the ground state) and TDDFT method (excitation spectra calculations) with the solvation models PCM-LR or PCM-SS, respectively. In particular, the SS approach is considered here for the lowest excited state of the solute with the solvent reaction field corresponding to its ground state. The DFT/TDDFT/PCM-SS(NEq) method represents nonstandard calculations of the fluorescence emission in which the molecular structure is optimized in the ground state (DFT/PCM method) whereas the fluorescence spectra are calculated by the TDDFT/PCM-SS method with the solvation reaction field relevant to the lowest excited state of the solute. This type of calculations indeed correspond to the case of the equilibrium solvation but non-equilibrium (unrelaxed) solute geometry. Obviously, this is a crude approach which nevertheless allows to understand an influence of the solvent reorganization alone on the electronic transitions, i.e. to separate it from the effects caused by a solute reorganization in polar environment. In contrast to it, the TDDFT/PCM-SS(Eq) method represents here one of the standard approaches where the molecular structure optimization in the excited state likewise the fluorescent spectra calculation is performed within the TDDFT/PCM-SS method. It thereby corresponds to the case when the solvent reaction field and the solute geometry in the excited state both reach their equilibrium, i.e. fully relaxed states prior to a further vertical electronic transition into the final non-equilibrium ground state. The combinations DFT/PCM/PM3/ORF or TDDFT/PCM/PM3/ORF represent hybrid approaches in which the molecular geometry is optimized by DFT/PCM (ground state, absorption process) or TDDFT/PCM (excited state, emission process) methods whereas the electronic spectra are calculated using the semiempirical method PM3 with further their correction within the solvation LM-ORF model.

All the methods properly predict the hypsochromic (blue) shift of the first absorption band and the bathochromic (red) shift of the fluorescence band while the solvent polarity rises from CHX to ACN. As far as the absorption process is concerned, pure DFT/TDDFT methods exhibit also rather good quantitative agreement regarding the spectral position of the first absorption band ($0 \rightarrow 0'$ transition). In all the cases the discrepancy between the experiment and theory is less than 0.1 eV. However, the magnitude of the solvatochromic shift appears to be somewhat overestimated compared to the measured one, namely by a factor of about 1.8 and 3.1 as for DFT/TDFT/PCM-LR and DFT/TDDFT/PCM-SS approaches, respectively. The hypsochromic trend of the first absorption band is also

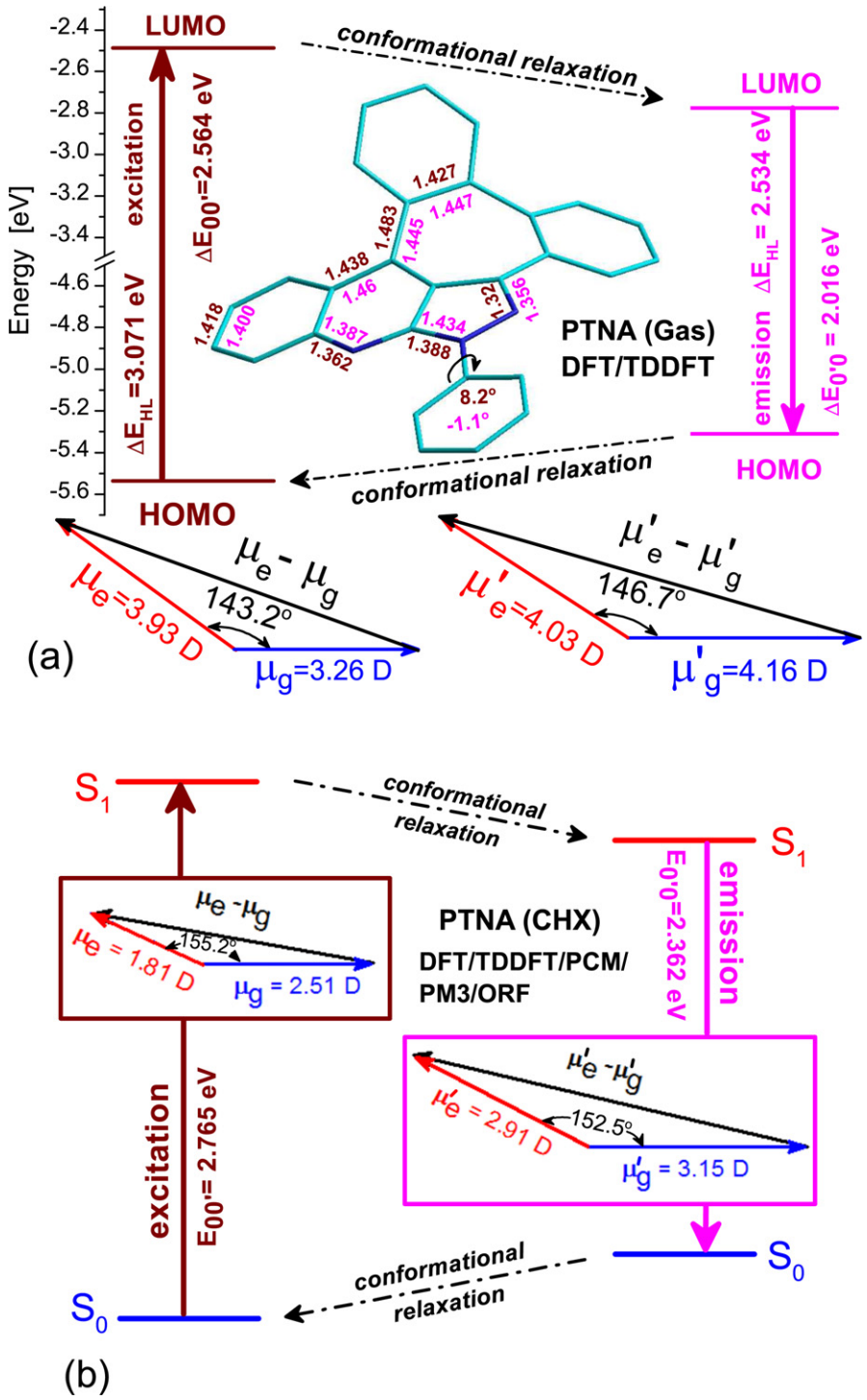

Fig. 6. (a) HOMO–LUMO energy levels, $0 \rightarrow 0'$ ($0' \rightarrow 0$) transition energies and vector diagrams at the vertical absorption (left) and emission (right) processes being calculated by DFT/TDDFT method for PTNA in the gas phase; in the central part the equilibrium molecular structure in the gas phase is shown. The torsion angle and several bond lengths are labeled for both absorption (equilibrium ground state geometry, wine color) and emission (equilibrium excited state geometry, magenta) processes. (b) $0 \rightarrow 0'$ and $0' \rightarrow 0$ transition energies and vector diagrams at the vertical absorption (left, wine color) and emission (right, magenta) processes, respectively, being calculated for PTNA by semiempirical PM3 method in combination with solvation LM-ORF approach (CHX solution); the molecular geometry has been optimized by DFT/PCM or TDDFT/PCM methods and further used as the input one in the semiempirical PM3/ORF calculations as for the absorption or emission processes, respectively. (For interpretation of the references to color in this figure legend, the reader is referred to the web version of the article.)

consistent with the vector diagram (see Fig. 6(a), left) presenting the spatial orientation of the ground ($\vec{\mu}_g$) and lowest excited ($\vec{\mu}_e$) state dipole moments in the gas phase while the vertical excitation of the solute from its ground state. An appropriate interpretation in this respect may be given within the ORF model [28] by means of the Lippert–Mataga [29,30] solvatochromic equations defining the transition energy in absorption ($E_{00'}$) or emission ($E_{0'0}$) processes as [31]:

$$E_{00'} = E_{00'}^{gs} - \frac{2\vec{\mu}_g(\vec{\mu}_e - \vec{\mu}_g)F(\varepsilon, n)}{a_0^3} \quad (1)$$

$$E_{0'0} = E^{gs}_{0'0} - \frac{2\vec{\mu}'_e(\vec{\mu}'_e - \vec{\mu}'_g)F(\varepsilon, n)}{a_0^3} \quad (2)$$

Here $F(\varepsilon, n) = (\varepsilon - 1)/(2\varepsilon + 1) - (n^2 - 1)/(4n^2 + 2)$ is the polarity of solvent expressed via its static dielectric constant ε and refractive index n; a_0 is the Onsager (cavity) radius; $E^{gs}_{00'}$ and $E^{gs}_{0'0}$ are the transition energies for the optical absorption or fluorescence emission in the gas phase ($F = 0$), respectively. The conformational relaxation in the excited state causes a modification of molecular properties thus, generally speaking, $E^{gs}_{00'} \neq E^{gs}_{0'0}$ likewise $\vec{\mu}_g \neq \vec{\mu}'_g$ and $\vec{\mu}_e \neq \vec{\mu}'_e$. This fact is usually ignored, however in many cases, particularly for PTNA, it appears to be important in the sense of accuracy related with further quantum-chemical evaluations. Evidently, the blue shift of the first absorption band likewise the red shift of the fluorescence band in a polar solvent environment ($F \neq 0$) are caused by a specific orientation of dipole moments $\vec{\mu}_g$ ($\vec{\mu}'_g$) and $\vec{\mu}_e(\vec{\mu}'_e)$, i.e. appear to be consistent with the opposite signs of the scalar products $\vec{\mu}_g(\vec{\mu}_e - \vec{\mu}_g)$ and $\vec{\mu}'_e(\vec{\mu}'_e - \vec{\mu}'_g)$, respectively, see vector diagrams in Fig. 6.

Fig. 4(b) presents the optical absorption spectra calculated by DFT/TDDFT/PCM-LR method. Herein blue, green and red colors correspond to CHX, THF and ACN solutions, respectively. The vertical lines are the oscillator strengths due to the electronic transitions between the singlet ground (S_0) and excited (S_i) states. The continuous lines simulate the spectra where the absorption bands are approximated by the Gaussian shape. The empirical parameter Γ has been chosen at the magnitude of 0.25 eV, which most properly describes actual bandshape broadening. Further methodology details regarding such type of calculation can be found e.g. in Refs. [1–4]. Comparing panels (a) and (b) in Fig. 4 one can see that DFT/TDDFT/PCM-LR method well reproduces the basic features of the measured spectra including the first absorption band in the visible range and the strongest band in the UV-region. However, the first absorption maximum, being calculated for several solvents, is slightly red shifted (25–30 nm) with respect to the measured one. The discrepancy should not be only attributed to the accuracy of DFT/TDDFT approach keeping also in mind that a vibronic coupling indeed has been ignored in such calculations. More adequate approach, presented in inserts of Fig. 4(b), considers the vibronic structure and thus more properly describes the shape of the first absorption band. Following Refs. [31–33] it has been modeled here via the vibronic series as:

$$A(E) \propto \frac{M_a^2 E}{\sqrt{4\pi h_0 k_B T}} \sum_{j=0}^{\infty} \frac{e^{-S} S^j}{j!} \exp\left(-\frac{(E - E_{00'} - jE_v)^2}{4h_0 k_B T}\right) \quad (3)$$

where $A = \log(I_0/I)$ is the absorbance, M_a is the transition moment corresponding to the vertical transition from the ground state, S is the vibronic coupling constant, $E = h\nu$ is the excitation energy, E_v is the vibronic energy spacing, k_B is the Boltzmann constant, T is the temperature. The reorganization energy h_0 is related to the low-frequency motions such as reorientation of the solvent shell (h_s) as well as any other low-frequency and medium-frequency nuclear motions of the solute (h_n). Accordingly, it may be presented by their sum as [31]:

$$h_0 = h_n + h_s = h_n + \frac{(\vec{\mu}_e - \vec{\mu}_g)^2}{a_0^3}\left(\frac{\varepsilon - 1}{2\varepsilon + 1} - \frac{n^2 - 1}{2n^2 + 1}\right) \quad (4)$$

In our calculations the values S, E_v and h_n have been considered as the model parameters. With the magnitudes $S = 1.2$, $E_v = 1300\ \mathrm{cm}^{-1}$ and $h_n = 0.125$ eV one gets the best agreement with the shape of the first absorption band being measured in weakly polar CHX solution. All other quantities of interest, like transition moment M_a, transition energy $E_{00'}$, ground state dipole moment $\vec{\mu}_g$ and excited state dipole moment $\vec{\mu}_e$ have been directly determined from DFT/TDDFT or DFT/TDDFT/PCM calculations. The Onsager radius, a_0, is taken to be equal to 0.552 nm as suggested by the molecular volume calculation within DFT method. By comparing inserts in Fig. 4(a) and (b) it is evident that DFT/TDDFT/PCM-LR method in combination with Eq. (4) practically perfectly reproduces the shape of the absorption band likewise the basic features of its solvatochromic behavior.

As for the fluorescence emission being considered the conformational relaxation of the solute in the excited state should be taken into account. Already in the gas phase it provides the red shift of the fluorescence emission. Fig. 6(a) demonstrates the absorption–emission cycle of PTNA in the gas phase including the energy and vector diagrams for both processes as calculated by DFT/TDDFT. Different colors, wine and magenta, correspond here to the vertical absorption from the equilibrium ground state and the vertical emission from the equilibrium excited state, respectively. Several bond lengths and the torsion angle, which defines the angular orientation of the phenyl group, are labeled for both states as well. Relaxation in the excited state leads generally to the elongation or shrinking of the bond lengths, keeping overall bent shape of the heteroazulene moiety practically unchanged. It is accompanied mainly by a rotation of the phenyl ring toward its nearly planar orientation in the gas phase and weakly polar CHX ($\phi = -1.2°$) or even slightly overcoming it in more polar solvents, as e.g. THF ($\phi = -7.9°$) or ACN ($\phi = -13.9°$). Nevertheless, even such moderate conformational changes result to a considerable reduction of the HOMO–LUMO gap likewise the transition energy corresponding to the fluorescence emission. The geometrical relaxation is also accompanied by some changes of the ground and excited state dipole moments as one may see from the vector diagrams shown in Fig. 6(a). The difference between the excitation and emission energies, expressed as $\Delta E^o_{af} = E^{gs}_{00'} - E^{gs}_{0'0}$, gives a rough idea about the scale of purely conformational changes that happen with the solute during the absorption–emission cycle. The magnitudes $E^{gs}_{00'}$ and $E^{gs}_{0'0}$ can be indeed estimated by extrapolating the spectral position of the optical absorption or emission bands into the region $F \to 0$. Using the experimental absorption and emission spectra shown in Figs. 4(a) and 7(a), respectively, one obtains $\Delta E^o_{af} \approx 0.12$ eV. The TDDFT analysis relevant to this case gives for the gas phase, $\Delta E^o_{af} \approx 0.55$ eV, suggesting thus on considerably stronger conformational changes in the excited state. What could be the reason for such discrepancy? As a possible scenario may be, in principle, the emission from the excited state being far from equilibrium. However, following our recent studies [2] the fluorescence emission of PTNA in organic solvents of different polarity is characterized by the lifetime in the range of 17–18 ns. Evidently, for the molecule in the excited state it is long enough to reach new equilibrium prior the fluorescence emission. More plausible explanation should likely refer to a quality of the geometrical optimization itself, especially for the excited states which generally speaking may be not so good as for the ground states. Such opinion has been also shared by official representatives of the Gaussian, Inc. developing the software being used in the present study. Following their opinion [34] the problem consists in a restricted number of accurate experimental investigations to be able to assess how reliable TDDFT geometries are, in contrast to the DFT optimization being developed basing on the extensive experimental data available for ground state geometries. Interestingly, that TDDFT/PCM-SS(NEq) calculations, which completely ignore the conformational relaxation in the excited state, give in comparison with the experiment an excellent agreement for highly and medium polar solvents, such as e.g. ACN and THF, and just a bit overestimated energy of the fluorescence emission, in weakly polar solvents only, as e.g. CHX for which the discrepancy between experiment and theory is less than 0.07 eV. This appears to be in contrast with TDDFT/PCM-SS(Eq) approach which considerably underestimates it resulting thereby in much worse agreement with the experiment, see Fig. 5. The

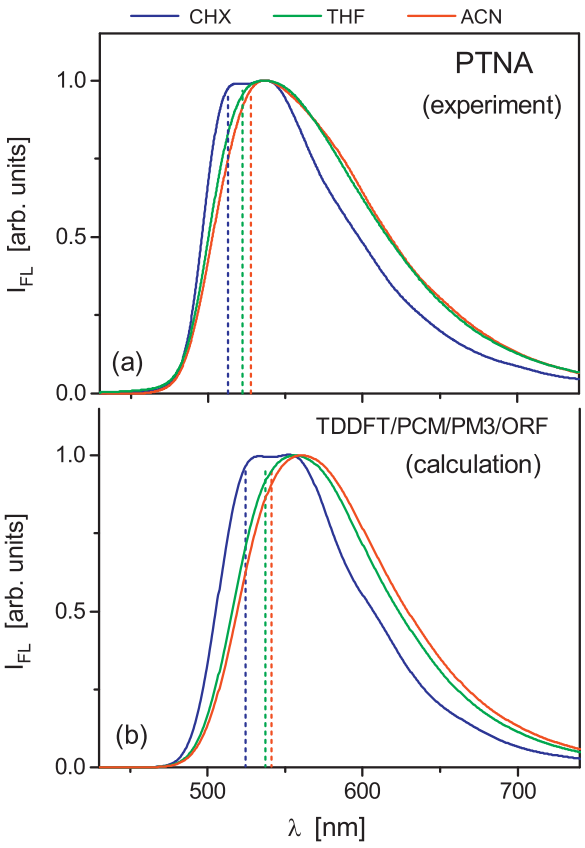

Fig. 7. The fluorescence spectra of PTNA in CHX (blue), THF (green) and ACN (red) solutions. (a) Measured spectra. (b) Calculated spectra by means of Eq. (5) with the set of model parameters $S = 1.2$, $E_v = 1300\,\mathrm{cm}^{-1}$, $h_n = 0.119\,\mathrm{eV}$ and the magnitudes $E_{0'0}$, $\vec{\mu}'_g$, $\vec{\mu}'_e$ being evaluated within the semiempirical PM3 method in combination with the solvation LM-ORF approach; the molecular geometry has been optimized for each solvent within the TDDFT/PCM method and used then as the input one in further semiempirical calculations; vertical broken lines indicate $0' \to 0$ transition. For the experimental data set [Section (a)] the transition $0' \to 0$ energies have been determined applying the band shape analysis by means of Eq. (5). (For interpretation of the references to color in this figure legend, the reader is referred to the web version of the article.)

discrepancy in the last case is about 0.45 eV. Accordingly, one may conclude that geometrical relaxation in the excited state, obtained within the TDDFT/PCM-SS(Eq) simulations, results to the conformational changes being likely considerably stronger than it is in reality. Roughly speaking, real equilibrium geometry in the excited state seems to be much closer to the ground state geometry, as obtained within the DFT optimization, rather than to the one which follows from the excited state geometry optimization using the TDDFT method. One may conclude that the dominant influence on the fluorescence emission in a solvent environment results mainly from the solvent reorganization in the excited state whereas the solute reorganization itself is indeed weak and has only a marginal meaning. Both TDDFT/PCM methods give the bathochromic shift of the fluorescence emission in accordance with the experimental observation as well as the vector diagram shown in Fig. 6(a). However, the magnitude of the solvatochromic coefficient, $dE_{0'0}/dF$ appears to be somewhat overestimated compared to the measured one, namely by a factor of about 1.3 or 2.1 as for TDDFT/PCM-SS(Eq) or TDDFT/PCM-SS(NEq), respectively.

A more deeper analysis of such discrepancy should consider also a specific of the B3LYP xc-potential used in TDDFT calculations. Despite its popularity in the organic chemistry several serious problems and critical remarks were addressed in respect to this method, see Ref. [35] and cited works there. It turned out that an application of B3LYP may lead to a severe underestimation of excitation energies in the charge transfer (CT) states [36] and, in general, its performance considerably drops down with increased system size [37,38]. The reason for this is usually addressed to the fact that B3LYP does not account for the long-range interactions. We obviously do not deal here with a large molecular system although some features indicating on a weak CT character related to the HOMO $\rightleftharpoons$ LUMO transition must be indeed admitted, see calculated HOMO and LUMO in Fig. 3. Amazingly that corresponding orbitals look quite similar for both excitation and emission processes and only the quantitative analysis basing on evaluated ground and excited state dipole moments [see Fig. 6(a)] recognizes certain differences here. Such differences are bonded to the different molecular geometries which characterize both processes in the absorption–emission cycle. For PTNA molecule it turns out that the excited state dipole moment at the vertical emission (optimized TDDFT geometry, S_1 state) appears to be only slightly larger compared to the one in the vertical absorption (optimized DFT geometry, S_0 state), $\mu'_e = 4.03$ D and $\mu_e = 3.93$ D, respectively. However, the difference is more pronounced if one compares the ground state dipole moments. It gives $\mu'_g = 4.16$ D and $\mu_g = 3.26$ D, respectively. Thus a challenging problem remains an answer on whether such moderate electron density relocation, which accompanies the geometry relaxation in the excited state, may so seriously impact the TDDFT calculations based on xc-potential B3LYP? We emphasize here the fact that TDDFT with such hybrid potential practically perfectly predicts the excitation energy of $S_0 \to S_1$ transition (the discrepancy is less than 0.02 eV) and exhibits evident failure only if the emission energy, associated with reverse transition $S_1 \to S_0$, is evaluated.

Applying so-called long-range-corrected (abbreviated as LC or LRC in the literature) approaches, e.g. LC-BLYP, one may shade more light on the problem. In contrast to conventional hybrid functionals incorporating a constant fraction of HF exchange, the LC methods mix HF exchange densities nonuniformly by partitioning the electron repulsion operator on a short-range interaction, $(1 - \mathrm{erf}(\omega r_{12}))/r_{12}$, which decays rapidly on a length scale of $2/\omega$, and the long-range part of the Coulomb interaction, $\mathrm{erf}(\omega r_{12})/r_{12}$ [35]. Here $r_{12} = |\mathbf{r}_2 - \mathbf{r}_1|$ is the interelectronic distance and ω is the damping (range-separation) parameter being sensitive to a size of molecule likewise a specific of the electron density distribution. For this reason parameter ω is adjustable for a particular molecular system. Moreover, in accurate evaluations it is adjusted sometimes even for particular states or electronic transitions being under consideration [39]. As for the molecule PTNA in the gas phase our DFT/TDDFT analysis with pure xc-potential LC-BLYP indeed shows different ω values for the absorption and emission processes, namely 0.14 Bohr^{-1} and 0.22 Bohr^{-1}, respectively. Assuming that ω is chosen at 0.14 Bohr^{-1}, which gives exact magnitude of the excitation energy, an underestimation in a prediction of the emission energy is then of about 0.36 eV, i.e. quite similar to the one obtained by DFT/TDDFT calculation with hybrid B3LYP potential. Further details regarding this analysis will be published elsewhere. This finding suggests that also in the case of LC methods even moderate modification of the electron density, due to e.g. geometry relaxation in the excited state, has strong impact on interelectronic interaction thus accurate evaluation of the transition energies requires reparameterization of xc-potential separately for the absorption and emission processes. On the other hand, the quality of the geometry optimization in the excited state maps to the same problem taking into account that the final (relaxed) geometry depends much on the form of the xc-potential, i.e. on the range separation parameter ω in a particular case of LC-BLYP method. Accordingly, the optimization process specifically for each particular excited state should be based on a self-consistent readjustment of ω in order to reach its optimized value in the end of the optimization procedure. Up to date

this obviously remains a quite challenging and unresolved problem in the quantum-chemical calculations.

Pretty good agreement with the experiment provides the hybrid approach being the combination of the TDDFT/PCM optimization with semiempirical calculations using PM3 method in combination with the solvation model LM-ORF (TDDFT/PCM/PM3/ORF approach). Fig. 6(b) shows the energy and vector diagrams obtained by this method for the vertical absorption and emission processes. In comparison with the DFT/TDDFT approaches, the semiempirical PM3 method gives smaller ground and excited state dipole moments, however their spatial arrangement is similar in both cases, i.e. it is consistent with the red shift of the fluorescence emission as the solvent polarity rises. With the cavity radius $a_0 = 0.43$ nm, as in Ref. [2], the hybrid model almost perfectly reproduces the energy of the fluorescence emission ($0' \rightarrow 0$ transition) as well as the magnitude of the solvatochromic shift itself, see Fig. 5. Moreover, a real shape of the fluorescence band due to vibronic coupling may be reproduced similarly as for the optical absorption, namely like as [31–33]:

$$I(E) \propto \frac{M_f^2 E^3}{\sqrt{4\pi h_0 k_B T}} \sum_{j=0}^{\infty} \frac{e^{-S} S^j}{j!} \exp\left(-\frac{(E - E_{0'0} + jE_v)^2}{4h_0 k_B T}\right) \quad (5)$$

where $I(E)$ is the fluorescence intensity, M_f is the fluorescence momentum. Fig. 7 compares the measured fluorescence spectra with the ones being calculated by means of Eq. (5). With the model parameters $S = 1.2$, $E_v = 1300\,\mathrm{cm}^{-1}$ and $h_n = 0.119$ eV as well as the calculated magnitudes $E_{0'0}$, $\vec{\mu}'_g$, $\vec{\mu}'_e$, as given for CHX solution in Fig. 6(b), the shape of fluorescence band in weakly polar CHX is almost perfectly reproduced. Importantly, that the same set of the model parameters also well describes the fluorescent spectra in more polar solvents, like THF or ACN, as it is evident from Fig. 7.

4. Conclusion

Taking together, we have presented here the DFT/TDDFT study on the electronic structure and spectral properties of the seven-membered annulated heteroazulene derivative PTNA by applying solvation PCM and LM-ORF approaches at the B3LYP/6-31+G(d,p) level of theory. The results of calculations are compared with the experimental optical absorption and fluorescence spectra as well as with the cyclic voltammetry measurements.

In the case of the excitation process, the DFT/TDDFT methods exhibit rather good quantitative agreement regarding the spectral position of the first absorption band; the discrepancy between the experiment and theory is less than 0.1 eV. As for the fluorescence emission being considered the TDDFT calculations underestimate the transition energy of about 0.45 eV. The discrepancy should be likely attributed to insufficient accuracy of the TDDFT optimization in the excited state. On the other hand, the TDDFT/PCM calculations, which completely ignore the conformational relaxation in the excited state, give in comparison with the experiment an excellent agreement in highly and medium polar solvents and just a bit overestimated energy of the fluorescence emission (of about 0.07 eV) in weakly polar solvents only. One may conclude that the dominant influence on the fluorescence emission in a solvent environment results mainly from the solvent reorganization in the excited state whereas the solute reorganization is indeed weak and has only a marginal meaning. In the polar solvent environment, all the TDDFT/PCM approaches give the bathochromic (red) shift for the fluorescence emission and the hypsochromic (blue) shift for the optical absorption in accordance with the experimental observation. However, the solvatochromic coefficients which characterize such shift appear to be somewhat overestimated compared to the measured ones.

Fairly good agreement with the experiment provides the hybrid approach being the combination of the TDDFT/PCM optimization with semiempirical electronic structure calculations by PM3 method and solvation model LM-ORF (TDDFT/PCM/PM3/ORF approach). As for the fluorescence emission this method predicts the transition energies in different solvents with the accuracy better than 0.06 eV. Such result is less important in the quantum-chemical respect due to the different basis sets or even models to be applied for the geometrical optimization and electronic structure calculations, however it may be of considerable practical importance for the physical and/or chemical engineering dealing with a development of new fluorescent materials for a broad range of applications. Similar studies on other heteroazulene derivatives would be quite desirable in order to verify real accuracy of such hybrid approach.

Acknowledgement

The calculations have been carried out in Wrocław Centre for Networking and Supercomputing (http://www.wcss.wroc.pl), grant no. 160.

References

[1] K.S. Danel, P. Gąsiorski, M. Matusiewicz, S. Całus, T. Uchacz, A.V. Kityk, Spectrochim. Acta A 77 (2010) 16.
[2] S. Całus, K.S. Danel, T. Uchacz, A.V. Kityk, Mater. Chem. Phys. 121 (2010) 477.
[3] P. Gąsiorski, K.S. Danel, M. Matusiewicz, T. Uchacz, A.V. Kityk, J. Lumin. 130 (2010) 2460.
[4] P. Gąsiorski, K.S. Danel, M. Matusiewicz, T. Uchacz, R. Vlokh, A.V. Kityk, J. Fluoresc. 21 (2011) 443.
[5] G. Mao, A. Orita, L. Fenenko, M. Yahiro, C. Adachi, J. Otera, Mater. Chem. Phys. 115 (2009) 378.
[6] J.-A. Cheng, C.H. Chen, H.-P.D. Shieh, Mater. Chem. Phys. 113 (2009) 1003.
[7] S. Całus, E. Gondek, A. Danel, B. Jarosz, M. Pokladko, A.V. Kityk, Mater. Lett. 61 (2007) 3292.
[8] E. Gondek, S. Całus, A. Danel, A.V. Kityk, Spectrochim. Acta A 69 (2008) 22.
[9] E. Gondek, I.V. Kityk, A. Danel, Mater. Chem. Phys. 112 (2008) 301.
[10] S. Liu, P. He, H. Wang, J. Shi, M. Gong, Mater. Chem. Phys. 116 (2009) 654.
[11] K.S. Danel, A. Wisła, T. Uchacz, ARKIVOC x (2009) 71.
[12] M.J. Frisch, G.W. Trucks, H.B. Schlegel, G.E. Scuseria, M.A. Robb, J.R. Cheeseman, G. Scalmani, V. Barone, B. Mennucci, G.A. Petersson, H. Nakatsuji, M. Caricato, X. Li, H.P. Hratchian, A.F. Izmaylov, J. Bloino, G. Zheng, J.L. Sonnenberg, M. Hada, M. Ehara, K. Toyota, R. Fukuda, J. Hasegawa, M. Ishida, T. Nakajima, Y. Honda, O. Kitao, H. Nakai, T. Vreven, J.A. Montgomery Jr., J.E. Peralta, F. Ogliaro, M. Bearpark, J.J. Heyd, E. Brothers, K.N. Kudin, V.N. Staroverov, T. Keith, R. Kobayashi, J. Normand, K. Raghavachari, A. Rendell, J.C. Burant, S.S. Iyengar, J. Tomasi, M. Cossi, N. Rega, J.M. Millam, M. Klene, J.E. Knox, J.B. Cross, V. Bakken, C. Adamo, J. Jaramillo, R. Gomperts, R.E. Stratmann, O. Yazyev, A.J. Austin, R. Cammi, C. Pomelli, J.W. Ochterski, R.L. Martin, K. Morokuma, V.G. Zakrzewski, G.A. Voth, P. Salvador, J.J. Dannenberg, S. Dapprich, A.D. Daniels, O. Farkas, J.B. Foresman, J.V. Ortiz, J. Cioslowski, D.J. Fox, Gaussian 09, Revision B.01, Gaussian, Inc., Wallingford CT, 2010.
[13] E. Gondek, A. Danel, B. Kwiecień, J. Nizioł, A.V. Kityk, Mater. Chem. Phys. 119 (2010) 140.
[14] E. Koścień, E. Gondek, M. Pokladko, B. Jarosz, R.O. Vlokh, A.V. Kityk, Mater. Chem. Phys. 114 (2009) 860.
[15] R. Improta, V. Barone, G. Scalmani, M.J. Frisch, J. Chem. Phys. 125 (2006) 054103.
[16] R. Improta, G. Scalmani, M.J. Frisch, V. Barone, J. Chem. Phys. 127 (2007) 074504.
[17] J. Tomasi, B. Mennucci, R. Cammi, Chem. Rev. 105 (2005) 2999.
[18] E. Koścień, J. Sanetra, E. Gondek, A. Danel, A. Wisła, A.V. Kityk, Opt. Commun. 227 (2003) 115.
[19] E. Koścień, J. Sanetra, E. Gondek, B. Jarosz, I.V. Kityk, J. Ebothe, A.V. Kityk, Spectrochim. Acta A 61 (2005) 1933.
[20] S. Calus, E. Gondek, A. Danel, B. Jarosz, A.V. Kityk, Opt. Commun. 268 (2006) 64.
[21] S. Całus, E. Gondek, A. Danel, B. Jarosz, A.V. Kityk, Opt. Commun. 271 (2007) 16.
[22] S. Trasatti, Pure Appl. Chem. 58 (1986) 955.
[23] V.V. Pavlishchuk, A.W. Addison, Inorg. Chim. Acta 298 (2000) 97.
[24] B.W. D'Andrade, S. Datta, S.R. Forrest, P. Djurovich, E. Polikarpov, M.E. Thompson, Org. Electron. 6 (2005) 11.
[25] A.R. Allouche, Gabedit is a Free Graphical User Interface for Computational Chemistry Packages. Available from: http://gabedit.sourceforge.net/.
[26] R.L. Martin, J. Chem. Phys. 118 (2003) 4775.
[27] E. Badaeva, V.V. Albert, S. Kilina, A. Koposov, M. Sykorad, S. Tretiak, Phys. Chem. Chem. Phys. 12 (2010) 8902.
[28] L. Onsager, J. Am. Chem. Soc. 58 (1936) 1486.
[29] E. Lippert, Z. Naturforsch. A 10 (1955) 541.
[30] N. Mataga, Y. Kaifu, M. Koizumi, Bull. Chem. Soc. Jpn. 28 (1955) 690.

[31] A. Kapturkiewicz, J. Herbich, J. Karpiuk, J. Nowacki, J. Phys. Chem. A 101 (1997) 2332.
[32] R.A. Marcus, J. Phys. Chem. 93 (1989) 3078.
[33] I.R. Gould, R.H. Young, L.J. Miller, A.C. Albrecht, S.J. Farid, J. Am. Chem. Soc. 116 (1994) 8188.
[34] F.R. Clemente, Private Communication (Technical Support Gaussian, Inc.), 31.03.2011.
[35] B.M. Wong, T.H. Hsieh, J. Chem. Theory Comput. 6 (2010) 3704.
[36] Y. Kurashige, T. Nakajima, S. Kurashige, K. Hirao, Y. Nishikitani, J. Phys. Chem. A 111 (2007) 5544.
[37] A. Dreuw, M. Head-Gordon, J. Am. Chem. Soc. 126 (2004) 4007.
[38] M.D. Wodrich, C. Corminboeuf, P.R. Schreiner, A.A. Fokin, P.v.R. Schleyer, Org. Lett. 9 (2007) 1851.
[39] B.M. Wong, M. Piacenza, F.D. Salab, Phys. Chem. Chem. Phys. 11 (2009) 4498.